J. Electrochem. Sci. Eng. **16** (2026) 3216; https://doi.org/10.5599/jese.3216

Open Access : : ISSN 1847-9286
https://pub.iapchem.org/ojs/index.php/JESE

Original scientific paper

Silver-doped TiO_2 nanotube array nanosensor for gallic acid detection: active surface and electrochemical enhancement

Zaira Mora-Mora[1], Ma. Guadalupe Garnica-Romo[2,✉], Héctor Eduardo Martínez-Flores[3], Juan José Alvarado-Gil[4] and Leandro García-González[5]

[1]*Programa Institucional de Doctorado en Ciencias Biológicas, Universidad Michoacana de San Nicolás de Hidalgo, Santiago Tapia 403, Col. Centro, C.P. 58000, Morelia, Michoacán, México*
[2]*Facultad de Ingeniería Civil, Universidad Michoacana de San Nicolás de Hidalgo, Santiago Tapia 403, Col. Centro, C.P. 58000, Morelia, Michoacán, México*
[3]*Facultad de Químico Farmacobiología, Universidad Michoacana de San Nicolás de Hidalgo, Tzintzuntzan 173, Col. Matamoros, C.P. 58240, Morelia, Michoacán, México*
[4]*Applied Physics Department, Cinvestav-Unidad Mérida, Carretera Antigua a Progreso Km. 6, Mérida, Yucatán 97217, México*
[5]*Universidad Veracruzana, Centro de Investigación en Micro y Nanotecnología, Veracruz, México*

Corresponding Author: ✉gromar05@hotmail.com

Received: January 12, 2026; Accepted: April 25, 2026; Published: May 8, 2026

Abstract

The development of electrochemical methods for the detection of phenolic compounds is a highly active area of research, motivated by their simplicity, efficiency and versatility of application. This work presents the synthesis and characterization of an electrochemical nanosensor for the detection of gallic acid, a phenolic compound of nutraceutical and analytical relevance. The nanosensor is based on a titanium electrode superficially modified with a titanium oxide nanotube array doped with silver (Ag-TNA). It was synthesized via electrochemical anodization and characterized using scanning electron microscopy, X-ray diffraction, Raman spectroscopy, and X-ray photoelectron spectroscopy. The electrochemical properties and gallic acid sensing capability were tested using electrochemical impedance spectroscopy and cyclic voltammetry. The results confirmed the obtention of an electrode surface composed mainly of titanium oxide in the anatase phase with the presence of oxygen vacancies. Metallic silver was found incorporated in interstitial form, while the ionic silver state is present superficially. The presence of silver promotes crystallinity and active surface area of the electrode. The Ag-TNA nanosensor displays two oxidation peaks in response to gallic acid; the first peak, registered at 1.3 V vs. Ag/AgCl, was used for the detection method developed in a linear range of 565 to 4663 µM (R^2= 0.997). Key analytical parameters were calculated, obtaining a sensitivity of 118 µA mM^{-1} cm^{-2}, limit of detection of 13.2 µM, limit of quantification of 43.9 µM, and relative standard deviation of 3.4 and 4.5 % in repeatability and reproducibility tests, respectively. The sensor exhibited selectivity toward glucose and ascorbic acid, common interferents.

Keywords
Applied electrochemistry, advanced nanomaterials, metal-doped nanotubes, phenolic acid, antioxidant determination

Introduction

Phenolic compounds (PCs) represent a substantial group of secondary metabolites found in fruits, vegetables, and medicinal plants. These compounds are recognized for their antioxidant and anti-inflammatory properties and their potential health benefits, particularly in the prevention of chronic degenerative diseases. The accurate detection of these compounds is of essential importance in a variety of fields, including food, pharmaceutical, and environmental sciences. In these fields, the quantification of these compounds is necessary for the control of product quality and authenticity, as well as for the evaluation of their impact on human health [1,2].

Among the PCs, gallic acid is distinctive due to its high antioxidant capacity, its presence in natural extracts, and its use as an analytical reference in assays of total antioxidant capacity and phenolic content. Furthermore, its incorporation into pharmaceutical and nutraceutical formulations has encouraged the development of specific, sensitive, reliable, and accessible methods for its determination [2-4].

In this context, electrochemical methods, complemented by advances in nanotechnology, have emerged as a promising alternative to traditional analytical techniques, particularly high-density liquid chromatography and spectroscopy. The technological sophistication of these tools, coupled with their rapid analysis capabilities and cost-effectiveness, makes them particularly well-suited for applications in quality control and online monitoring. This suitability extends to educational contexts as well [3,5,6]. The most widely studied electrode/sensor materials for electrochemical sensing applications include graphite sheets (GSs) or rods (PGEs) [7,8], carbon glass electrode (GCE) [9], carbon paste electrode (CPE) [10], gold [11], platinum [12], and indium tin oxide (ITO) [13]. The performance of all these electrodes has been enhanced through surface modification with metal nanoparticles, carbon nanotubes, graphene [14], quantum dots [15], metal oxides [16], or hybrid combinations functionalized with polymers, enzymes, or other biomaterials [2,17,18,19]. These sensors have demonstrated high levels of sensitivity, reaching detection limits in the micromolar and even nanomolar range. This makes them promising analytical tools for quality control applications in the fields of food, pharmaceuticals, the environment, and clinical analysis [6].

However, some of their limitations include the loss of long-term operational stability, loss of response after some cycles of use, the high cost of certain nanomaterials used in electrode modification, and the complexity of some fabrication processes [3-6]. As an example, we can mention the gallic acid (GA) sensor developed by Falahi *et al*. [4], based on a 3D bio-nanocomposite of multi-walled carbon nanotube and atacamite as a modifier of the CPE. Gao *et al*. [20] presented a GA sensor using chitosan and reduced graphene oxide (ERGO). Gu *et al*. [21] used a glassy carbon electrode modified with a nanocomposite of silicon oxide and carbon nanotubes to detect GA. These sensors showed sensitive determination of GA and a limited long-term stability, reporting a loss of sensitivity of 13 % in 30 days, 6 % in 7 days, and 13.4 % in 15 days, respectively. The exploration of novel materials remains imperative to enhance stability, reduce manufacturing costs, and adapt sensing platforms to diverse application contexts, ranging from laboratories to portable or on-site systems. In this regard, the selection and design of the sensing material constitute a key aspect in achieving specific objectives, in accordance with the requirements of the analyte and the application environment [8].

Particularly in the field of electrochemical nanosensor development, anodic titanium dioxide nanotube arrays (TNAs) have the potential to be high-performance electrochemical receptor-

transducers that are low-cost, chemically stable, and compatible with aqueous media, making them attractive for analytical applications thanks to the synergy between the semiconductor and the catalytic properties of titanium dioxide TiO_2 and the ordered nanotubular morphology that enhances conductivity [22,23]. The properties of nanostructured TiO_2 have been successfully used with excellent results in the construction of solar cells [24], lithium batteries [25], biosensors and nanosensors [22], and pollutant degradation [26], among others. TiO_2 nanoparticles (TiO_2 NPs) have been the most studied; however, TiO2 nanowires (NHs), nanosheets (NLs), and nanotubes (NTs) are also obtainable. Depending on the synthesis method used, the nanotubes can grow randomly, forming powders, or in highly ordered arrays (TNAs) with perpendicular orientations to the substrate.

There are many advantages to using nanotube arrays (TNAs) over other morphologies for electrochemical sensing devices. For example, it is possible to highlight a larger specific area, as was reported by Chikere *et al*. [27]. They modified a CPE electrode with cobalt oxide nanoparticles, resulting in an active area three times that of the unmodified CPE. The tubular morphology of TNAs facilitates direct electron transport, thereby enhancing electrical conductivity, while their highly ordered structure minimizes agglomeration, a common issue in nanoparticle-based electrodes. Furthermore, TNAs grown in situ on a titanium substrate exhibit strong adhesion, eliminating the need for additional immobilization steps for their integration onto the electrode surface. This robust adhesion prevents crack formation and detachment of the nanostructures, thereby improving the overall stability of the system [22,28].

For the synthesis of TNAs, electrochemical anodization (EA) has established itself as the most effective and versatile methodology for obtaining ordered arrays directly bonded to titanium metal substrates, simplifying the manufacturing process, as it does not require the use of binders or a subsequent step to bond it to the electrode base [29,30]. This technique allows key morphological parameters, such as the diameter and length of the nanotubes, to be controlled by adjusting electrolyte conditions, voltage, and anodization time [22,31,32]. Their ordered structure and high surface area facilitate interactions with electroactive species, promoting charge-transfer processes [33]. Another significant advantage of anodization is the ability to incorporate dopant metal species, such as gold, nickel, iron, and silver, directly into the array during synthesis. This single step not only simplifies the experimental procedure but also promotes homogeneous distribution and better structural integration of the dopant [30].

Silver-doped TiO_2 nanotube arrays (Ag-TNA) represent an attractive platform due to their combination of chemical stability, catalytic, and antimicrobial properties. This is because silver provides additional benefits, including increased electrical conductivity, improved charge-transfer efficiency, and the generation of active catalytic sites [34,35]. These properties are particularly relevant in electrochemical sensors for phenolic acid analytes, where oxide-reduction interaction can be enhanced by synergistic effects between TiO_2 semiconductor properties, its ordered nanotubular morphology and the increased catalytic sites [22].

In this context, the objective of this work is to develop and evaluate an electrochemical nanosensor based on a silver-doped TiO_2 nanotube array synthesized via a simple single-step anodization process. To the best of our knowledge, this specific structural configuration has not been previously reported for gallic acid detection, and its electrochemical performance is assessed in terms of interfacial properties, including active surface area and charge transfer resistance, as well as analytical parameters such as sensitivity, detection limit, and stability.

Experimental

Materials and reagents

To carry out this study, the following materials and reagents (all of analytical grade, purity >99 %) were used: titanium sheet (thickness 0.127 mm) (Sigma-Aldrich, Mexico), silicon carbide abrasive paper (Fandeli, Mexico), acetone (Golden Bell, Mexico), methanol (J.T. Baker, Mexico), hydrochloric acid and ammonium fluoride (Fermount, Mexico), monoethylene glycol, isopropanol, silver nitrate, potassium chloride, potassium ferrocyanide, gallic acid, and glucose (Meyer, Mexico), and deionized water (Tecnología y control Ambiental, Mexico).

Electrode preparation

Two types of electrodes were prepared by surface modification of titanium sheets (20×15 mm): one electrode based on TiO_2 nanotube array (TNA) and another based on a silver-doped TiO_2 nanotube array (Ag-TNA). The TNA electrode was used as a reference to compare the impact of doping on electrode characteristics and electrochemical performance.

The nanotube arrays (NA) were synthesized by electrochemical anodization, following the methodology used by Garnica-Romo *et al*. [36], with some modifications, mainly the increase in the percentage of the dopant precursor. This methodology consisted of pre-treating the titanium substrate (Ti), which includes unidirectional mechanical cleaning with silicon carbide sandpaper with grit sizes of 400, 600, 1200, 1500 and 2000, followed by chemical cleaning by ultrasonic bath with solvents (acetone, methanol, isopropanol, and deionized water), reducing the exposure time to 10 minutes *per* solvent. Subsequently, to remove solvent residues, the substrate was immersed in a solution of HCl (0.1 M) for 10 s, rinsed with deionized water, and left to air dry. Once clean, the substrates were exposed to the anodization process for 45 minutes at a potential of 30 V supplied by an external direct current power source (Wanptek P1030) in a base electrolyte composed of 90 vol.% monoethylene glycol and 10 vol.% deionized water, to which ammonium fluoride (0.5 wt.%) was added as a promoter of nanotube formation and silver nitrate (10 wt.%) as a precursor of the dopant. The silver nitrate was omitted during the synthesis of the TNA electrode. The process was carried out at room temperature and without pH adjustments. After anodization, the samples were rinsed with deionized water. They were then left to air-dry and subjected to heat treatment by calcination at 500 °C for 2 h to promote crystallization.

Characterization

It is widely known that the performance of a nanosensor depends on its electrochemical properties, which are closely linked to its crystal structure and surface composition [37]. The crystal structure was analysed by XRD using a Bruker D-8 Advance diffractometer with Cu-Kα_1 radiation (λ = 0.15405 nm) in grazing incidence configuration. The 2θ scan was performed from 20 to 80°, with a step size of 0.02° and an integration time of 0.5 s *per* step. In addition, the molecular vibration characteristics of the material were identified using Raman spectroscopy performed on a WITec Alpha 300R confocal microscope, with a 488 nm (10 mW) source, an exposure time of 2 s, and 20 accumulations, in the range of 100-900 cm^{-1}. The surface composition was determined by XPS, performing a general scan (0 to 1350 eV) with a step size of 1 eV and a step energy of 100 eV, followed by high-resolution (HR) scans in specific regions for the present elements. The analysis was performed on a Thermo Fisher Scientific K-Alpha instrument equipped with a monochromatic Al Kα (1486.6 eV) source operated at 12 kV and 40 W, with an oval irradiation footprint of 400 µm in diameter and an incidence angle of 30°.

Electrochemical evaluation

The electrochemical evaluation was carried out in two stages. The first consisted of surface characterization tests to evaluate the electrochemical response of electrodes based on pure TiO_2 nanotube (TNA) and silver-doped (Ag-TNA) arrays. The second stage involved developing the sensing method, including optimizing experimental parameters, constructing the calibration curve, and validating the analytical method using the Ag-TNA electrode.

In all tests, a potassium chloride (1 M KCl) solution was used as the supporting electrolyte and a three-electrode cell system consisting of the working electrode (Ti substrate, and TNA or Ag-TNA electrode, with an exposure area of 1 cm^2), an Ag/AgCl (3 M KCl) reference electrode, and a platinum auxiliary electrode. The techniques used were electrochemical impedance spectroscopy (EIS) and cyclic voltammetry (CV), both performed on a Gamry Instruments potentiostat (PC14 - 750). The EIS measurements were performed over the frequency range 10^5 Hz to 0.01 Hz under open-circuit conditions with a disturbance potential amplitude of 5 mV. For the CV analyses, different experimental parameters were applied depending on the analyte under study (potassium ferrocyanide or gallic acid).

The first stage of electrochemical characterization included EIS and CV tests with two analytes: potassium ferrocyanide ($K_4[Fe(CN)_6]$, 5 mM in 1 M KCl) used as a standard model compound, and gallic acid (GA, 5 mM in 1 M KCl) as the main analyte of interest in this work. These tests aimed to evaluate aspects such as the reversibility of the redox process on the electrode surface and the type of kinetic control (capacitive or resistive) and to demonstrate the response of the electrode to different analytes. The charge transfer resistance (R_{ct}) was determined by fitting an equivalent electrical circuit (EEC) model to the experimental impedance data. On the other hand, the CV analyses included tests over a wide range of potentials to identify the active zone and scan-rate tests, the results of which were used to calculate the electrochemically active area (A_{ECSA}) and surface charge density using the Randles-Ševčik equation.

For the second stage, all proofs were carried out using only the GA analyte and the Ag-TNA electrode to develop the sensing method. The optimal working parameters were determined by evaluating 5 mM GA solution, and tests were performed at scan rates (20, 40, 60, 80, 100, 120, 140 and 160 mV s^{-1}), pH (range of 2-6), temperature (10, 15, 22 and 30 ℃), and the maximum oxidation potential was identified. Subsequently, the calibration curve was constructed, starting from the analysis of the blank solution consisting of 35 mL of 1 M KCl, to which aliquots of the 50 mM GA stock solution were progressively added to form a range of 0 to 4663 mM. A linear range of the method was also obtained. Finally, the developed method was validated.

Results and discussion

Surface characteristics

The morphological characterization carried out using scanning electron microscopy with energy-dispersive X-ray spectroscopy (SEM-EDS) analysis (Figure 1) shows well-ordered TiO_2 nanotube arrays with Ti and O uniformly distributed in both TNA (Figure 1a) and Ag-TNA (Figure 1b). In the Ag-doped sample (Figure 1b), the EDS results also indicate an average Ag content of about 0.35 at. % and surface deposits reaching approximately 18 at.% in localized superficial areas. The elemental maps confirm that Ag is incorporated on the nanotube walls and surface without affecting the tubular morphology.

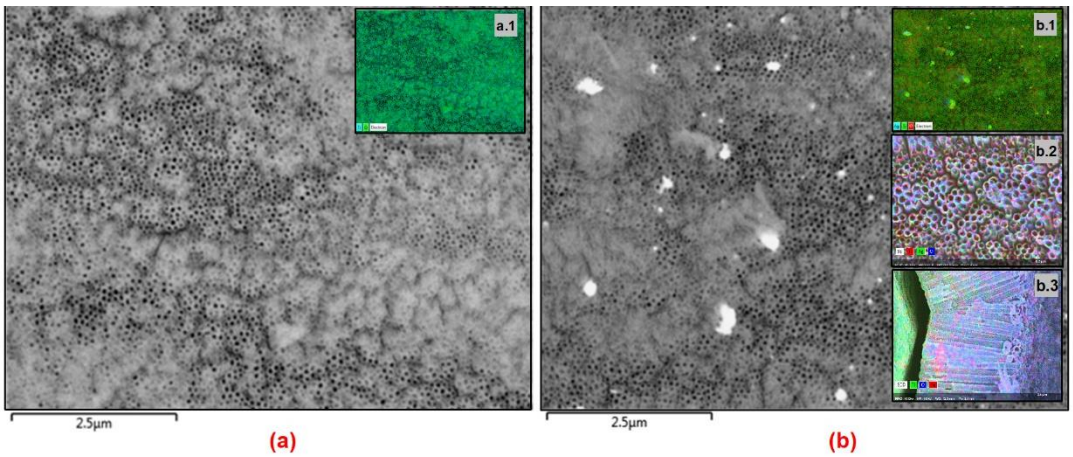

Figure 1. *SEM-EDS frontal views of (a) TNA and (b) Ag-TNA, each with its corresponding elemental map (insets a.1 and b.1). Additional insets in (b) show a higher magnification frontal map (b.2) and a cross-sectional map (b.3)*

The structural characteristics are presented in the XRD diffractograms of Figure 2, corresponding to the titanium foil substrate (Figure 2a) and the synthesized TNA and Ag-TNA samples (Figure 2b and 2c). The Ti diffractogram shows diffraction peaks at angles 2θ: 35.04, 38.2, 40.04, 52.92, 62.84, 70.56, 76.22 and 77.44°, which were identified with the planes (100), (002), (101), (102), (110), (103), (112) and (201) corresponding to the hexagonal structure of metallic titanium (PDF-04-001-8963, ICDD). These titanium diffraction peaks remain in the TNA and Ag-TNA samples, since the titanium foil serves as the substrate and supports the nanotube arrays.

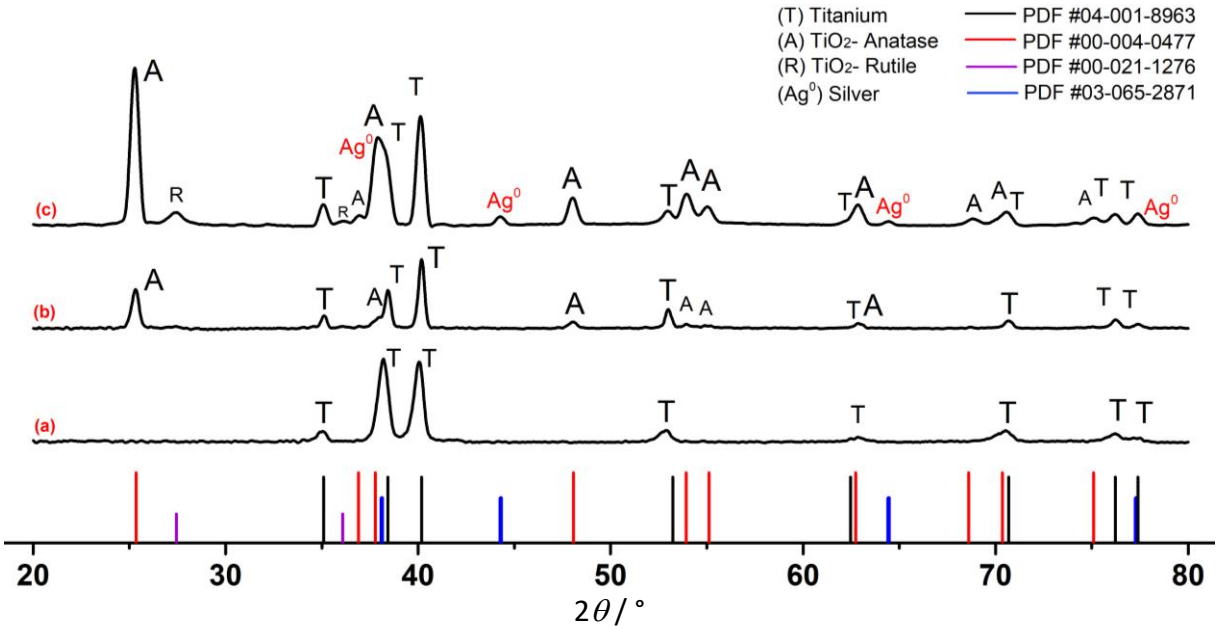

Figure 2. *XRD diffraction patterns of samples: (a) Ti, (b) TNA and (c) Ag-TNA*

The TNA sample (Figure 2b), in addition to the peaks attribute to metallic Ti, showed diffraction peaks at 25.32, 38.08, 48.08, 54.0, 55.16 and 63.02°, typical of TiO_2 in the anatase phase with a tetragonal structure (PDF-00-004-0477, ICDD), corresponding to the crystallographic planes (101), (004), (200), (105), (211) and (204), respectively.

Ag-TNA sample (Figure 2c) also has peaks from the Ti substrate, and for the anatase phase presents the peaks at 25.28, 36.9, 38.02, 48.08, 53.96, 55.16, 62.88, 68.8, 70.56 and 75.12°. These peaks are observed slightly shifted to lower angles and with greater intensities, indicating an

increase in crystallinity. Moreover, the peaks present at 27.4 and 36.04° are attributed to the onset of the rutile phase (PDF 00-021-1276, ICDD), and the peaks at angles of 37.90, 44.30 64.46 and 77.40° were identified as metallic silver (Ag^0) according to PDF file 00-043-0997.

The presence of silver in the Ag^0 state suggests that it is not part of the TiO_2 lattice, but rather is found in an interstitial form, attributed to the fact that the ionic radii of Ti and Ag are 68 pm and 126 pm, respectively, which does not allow it to occupy a site in the oxide lattice [38,39].

On the other hand, to determine the effect of the dopant on the degree of crystallinity of the samples, an analysis was performed by integrating the XRD diffraction patterns, resulting in a crystallinity of 75 and 85 % for the TNA and the Ag-TNA samples, respectively, indicating that the presence of silver encouraged a 10 % increase in crystallinity in the Ag-TNA compared to the TNA. These results indicate that the presence of the dopant precursor ($AgNO_3$) during the synthesis of TiO_2 nanotube arrays favour the crystallization of TiO_2, mainly the anatase phase, as obtained by Garnica-Romo *et al.* [36]. In addition, silver promotes the generation of nucleation centres for the initiation of rutile phase formation under the calcination treatment applied. This is related to the Ag precursor percentage used in this work and agrees with the results obtained by Viet *et al.* [39].

To further support the structural analysis, the spectra obtained from Raman spectroscopy are shown in Figure 3. The Ti substrate (Figure 3a) does not exhibit any Raman signal, while the anodized samples (TNA and Ag-TNA) display six active modes characteristic of the anatase phase of TiO_2, confirming XRD results. In the undoped TNA sample (Figure 3b), bands are observed at approximately 147 (Eg), 201 (Eg), 398 (B_{1g}), 518 (A_{1g}/B_{1g}) and 638.6 cm^{-1} (Eg), while in the doped sample Ag-TNA (Figure 3c) these bands appear at approximate values of 150, 203, 401, 518 and 638.6 cm^{-1}. These results show a slight shift towards higher band frequencies in Ag-TNA compared to TNA, attributed to the presence of silver, possibly because, as it is not found within the titanium oxide network, it induces stresses that increase vibrational frequency. The TNA sample only shows the vibration modes associated with the anatase phase. However, in the Ag-TNA sample, broadening of the B_{1g} band (401 cm^{-1}) and the Eg band (638.6 cm^{-1}) of the anatase phase is observed. This is due to the onset of rutile phase crystallization, which coincides with what was discussed in the XRD results [40].

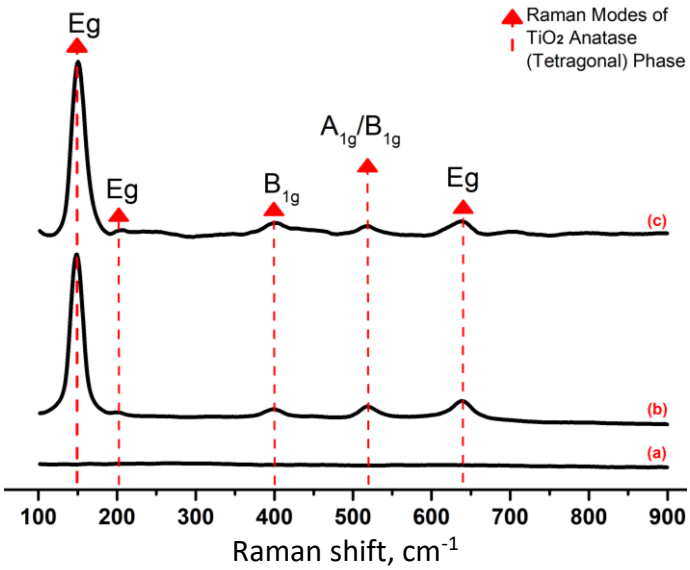

Figure 3. *Raman analysis of samples: (a) Ti, (b) TNA, and (c) Ag-TNA*

Complementing the characterization of structure and composition, the results of the XPS surface composition analyses are shown in Figure 4.

In the full scan of both TNA and Ag-TNA samples (Figure 4a), the elemental presence of Ti and O was determined, and Ag was also found in the Ag-TNA sample. The results of the high-resolution (HR) XPS scans for Ti showed two main peaks at 458.8 and 464.6 eV, for O, a main peak at 530.8 eV, and for Ag, two peaks at 373.68 and 367.68 eV. However, these peaks have an asymmetrical shape, so deconvolution analysis was performed, and the results are described below.

In the TNA sample, the HD spectrum of titanium (Ti 2p, Figure 4b) shows a doublet Ti $2p_{3/2}$–Ti $2p_{1/2}$ doublet at 458.8 and 464.5 eV, respectively, whose spin-orbit separation of 5.7 eV is attributed to the Ti^{+4} cation involved in the O–Ti–O network bonds [33]. A second doublet of lower intensity associated with partially reduced states of Ti (Ti^{+3}) due to oxygen vacancies or defects in the structure, with a signal recorded at 462.8 to 457.27 eV (Δ = 5.5 eV). The high-resolution (HR) scan of O (Figure 4c) yielded three signals (530.1, 531.2 and 531.76 eV), which are attributed respectively to O–Ti bonds (the most intense peak), oxygen absorbed on the surface (O_{ads}) probably bound to defects (Ti^{+3}) or silver, and finally to surface hydroxyl groups (–OH).

The high-resolution (HR) XPS spectra of Ti and O from the Ag-TNA sample (Figure 4e-f) exhibit similar results to TNA. Regarding Ti, a majority contribution from the doublet is attributed to Ti^{+4} of the TiO_2 network, and the presence of Ti^{+3} was also detected. In the case of O, contributions related to O–Ti, O_{ads}, and the presence of –OH were also obtained by deconvolution. Although the signals detected in TNA and Ag-TNA are indicative of the same oxidative states of the elements present, the Ag-TNA sample shows more intense signals, which could be due to greater crystallinity, as determined by XRD.

About silver, both metallic silver (Ag^0) and ionic silver (Ag^+) were identified, the latter being the most intense. The signals were determined by deconvolution of the HR XPS spectrum (Figure 4d), yielding two Ag 3d doublets, first at 368.6 to 374.9 eV (Δ=6.3 eV) attributed to Ag^0, and the other located at 367.66 to 373.69 eV (Δ=6 eV) attributed to Ag^+.

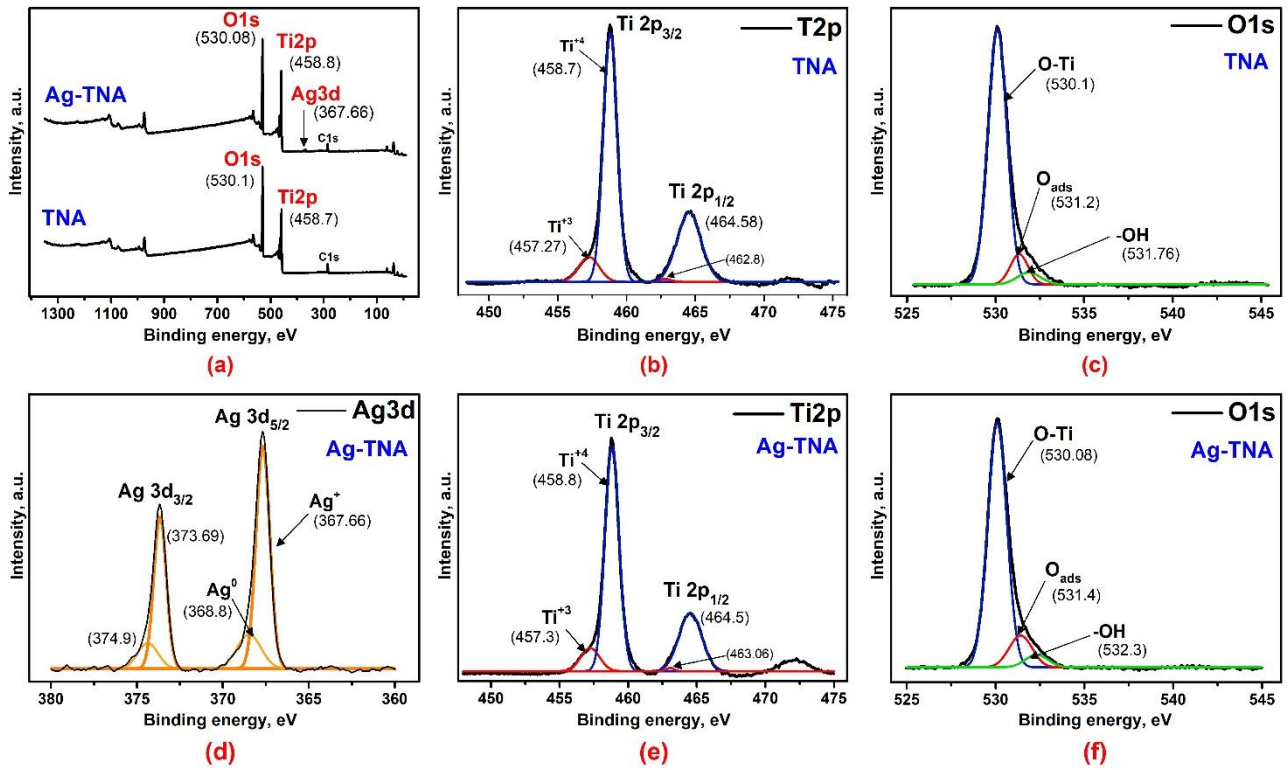

Figure 4. *XPS analysis: (a) full scan from 0-1300 eV of TNA and Ag-TNA samples, (b-c) high-resolution spectra of Ti and O from the TNA sample, (d-f) high-resolution spectra for Ag, Ti, and O, respectively, from the Ag-TNA sample*

These XRD and XPS results suggest that the TiO_2 matrices contain Ag^0 incorporated interstitially in the crystal lattice, while a higher concentration of Ag^+ is found on the surface, which could generate a synergistic effect that favours the sensing mechanism, on the one hand, the reduction of electron-hole recombination by the action of Ag^0, and, on the other hand, greater interaction and adhesion with the analyte by Ag^+.

Surface electrochemical properties

Figure 5 summarizes the results of the EIS and CV analyses of Ti, TNA, and Ag-TNA electrodes in response to a standard potassium ferrocyanide analyte. In the EIS analysis (Figure 5a), TNA, and Ag-TNA electrodes showed an area governed by capacitive and resistive contributions (semicircle) and a second area with diffusional contribution at low frequencies (Warburg effect). Both an increase in capacitance and a decrease in resistivity are observed for the Ag-TNA electrode compared to TNA, indicating that the presence of the dopant (Ag) increases surface area and conductivity. An equivalent electrical circuit (sketched in Table 1) was fitted to the experimental impedance data, yielding values for electrolyte resistance (R_s), charge transfer resistance (R_{ct}), constant phase element (CPE_{dl}, representing non-ideal capacitive response of the electrochemical interface), and Warburg impedance (W), associated with mass transport limitations by diffusion), as summarized in Table 1.

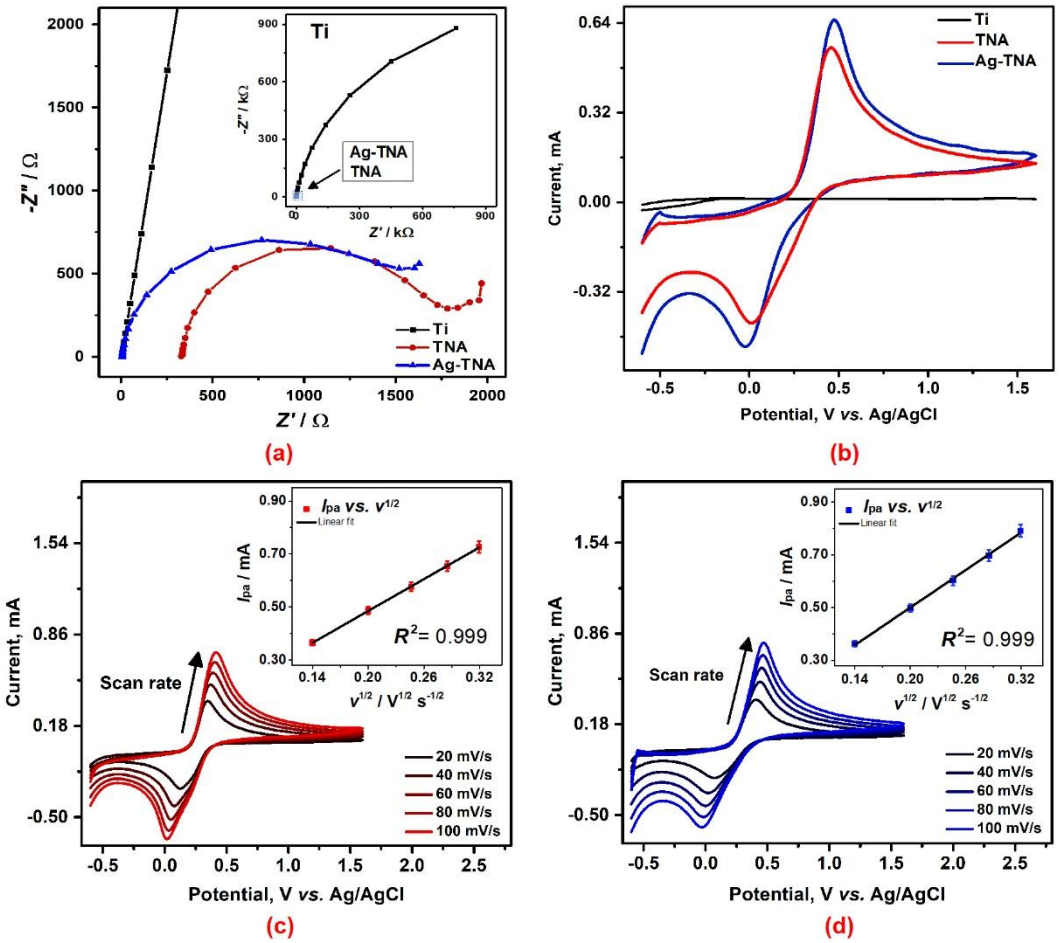

Figure 5. *Standard electrochemical tests with potassium ferrocyanide (5 mM in 1 M KCl): (a) impedance and (b) voltammetric response of Ti, TNA, and Ag-TNA electrodes at a scan rate of 100 mV s^{-1}; (c) and (d) effect of the scan rate on CVs of TNA and Ag-TNA electrodes, respectively. The insets show the relationship between anodic peak current (I_{pa}) and the square root of scan rate ($v^{1/2}$)*

On the other hand, Figure 5b shows the voltametric response of the tests with a ferrocyanide standard of the electrodes. The Ti electrode shows no response, while the TNA and Ag-TNA

electrodes register an anodic and a cathodic peak, indicating reversibility. However, the separation between peaks (ΔE_p) and the inequality between anodic and cathodic peak intensities ($I_{pa}/I_{pc}\neq1$) suggest a quasi-reversible profile.

Furthermore, consistent with the EIS results, the Ag-TNA electrode exhibits greater detection sensitivity at higher I_{pa} than TNA. The quasi-reversible profile was corroborated by scan-rate effect tests (Figure 5c-d), in which the anodic peak intensity (I_{pa}) shifts to higher overpotentials as the rate increases, suggesting a diffusion-limited kinetic profile. The electrochemically active area (A_{ECSA}) of the TNA and Ag-TNA electrodes was calculated from the experimental data of the scan rate tests (I_{pa} *vs.* $v^{1/2}$) using the Randles-Ševčik equation (1):

$$I_{pa}= (2.69x10^5)n^{3/2}A_{ECSA}\,D^{1/2}C\,v^{1/2} \quad (1)$$

where I_{pa} / A is the anodic peak current, n is the number of electrons transferred, A_{ECSA} / cm^2 is the electroactive surface area, D / $cm^2\ s^{-1}$ is the diffusion coefficient, C / mol cm^{-3} is the analyte concentration and v / V s^{-1} is the potential scan velocity.

The obtained values of A_{ESCA} are presented in Table 1.

Table 1. *Electrochemical properties of TNA and Ag-TNA electrodes evaluated using potassium ferrocyanide as a redox probe (5 mM in 1 M KCl)*

Sensor	Equivalent electrical circuit	R_s / Ω	R_{ct} / Ω	Q_{dl} / $m\Omega^{-1}\ s^n$	n	Q_W / $m\Omega^{-1}\ s^{0.5}$	A_{ECSA} / cm^2
TNA	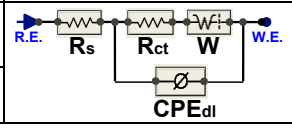	329	1412	0.604	0.920	7.91	0.00086
Ag-TNA		6.2	1344	0.770	0.936	7.02	0.00107

R_s: solution resistance; R_{ct}: charge transfer resistance; Q_{dl}: constant phase element (CPE_{dl}) parameter; n: CPE_{dl} exponent; Q_w: parameter of the CPE (n = 0.5) that models Warburg-type diffusive behaviour (W); A_{ECSA}: electrochemically active surface area

Gallic acid detection

Figure 6 shows the oxidation response of gallic acid at Ti, TNA and Ag-TNA electrodes. The CV spectra recorded in a 5 mM gallic acid (GA) solution exhibit significant changes compared to those obtained with the standard potassium ferrocyanide probe (Figure 5b), shifting from a quasi-reversible to an irreversible profile.

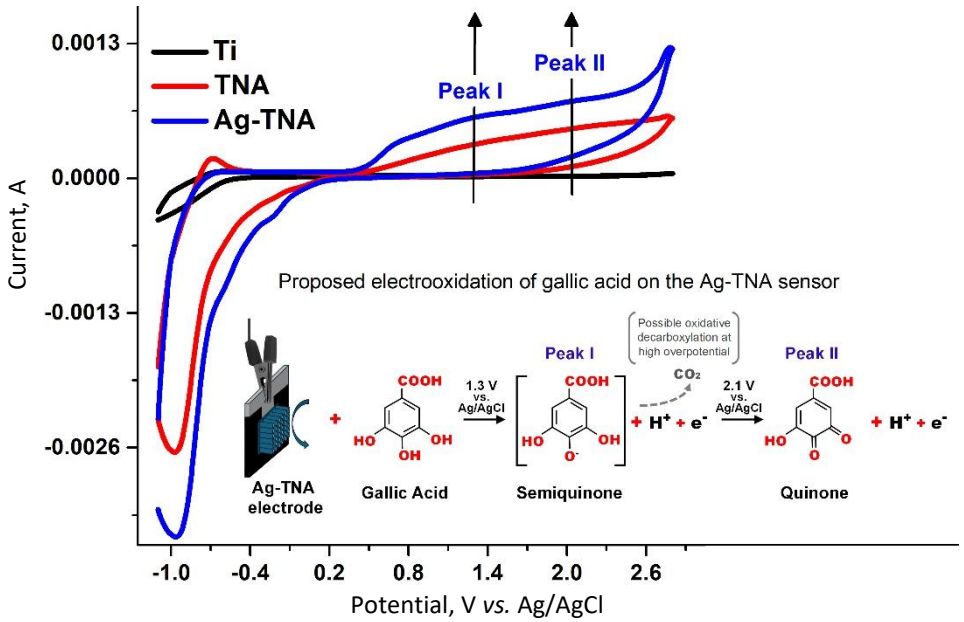

Figure 6. *Comparative CV curves of Ti, TNA, and Ag-TNA electrodes for the detection of 5 mM gallic acid in 1 M KCl (22 °C, pH 2). Inset: proposed electrooxidation behaviour of gallic acid on the Ag-TNA electrode, adapted from S. Falahi et. al. [4] and S. Lisnund et al. [41]*

Only TNA and Ag-TNA electrodes display an oxidation signal, while the Ti electrode shows no detectable response. The Ag-TNA electrode maintains higher sensitivity than TNA, with an approximate increase of 38 % in peak current.

In contrast to the standard redox probe evaluation, the analysis of gallic acid required extending the potential window up to 2.6 V to observe the complete oxidation behaviour. Additionally, scanning toward negative potential was necessary to maintain surface activation and minimize possible surface saturation effects. In most reports, the oxidation of GA typically occurs at potentials below 1.0 V using carbon-based electrodes [42]. However, in the present TiO_2 nanotubular/Ti system, two anodic peaks (I_{pa}) were identified at approximately 1.3 and 2.1 V, respectively. This positive shift may be attributed to the distinct surface chemistry and electronic properties of the semiconducting TiO_2 nanotubular matrix and the titanium substrate, as well as to the highly porous structure.

This behavior is consistent with literature reports describing the appearance of two oxidation signals [4,41]. The first peak at 1.3 V (peak I) is associated to the primary oxidation of gallic acid leading to semiquinone species, while the second peak at 2.1 V (peak II) is associated with further oxidation toward quinone formation. However, considering that oxidative decarboxylation of the –COOH group has been reported to occur at potentials close to 2.0 V in phenolic systems [43], the contribution of partial decarboxylation under high overpotential conditions cannot be excluded. Therefore, the process observed at peak II may involve simultaneous contributions from further oxidation and possible CO_2 evolution. Based on this signal definition, peak I at 1.3 V was selected as the analytical signal for the GA quantification method. The proposed oxidation pathway of gallic acid on the Ag-TNA electrode is illustrated in the inset of Figure 6.

Sensing parameters, calibration curve and method validation

After confirming the improved electrochemical performance of the Ag-TNA electrode compared to TNA, the Ag-TNA electrode was used in subsequent tests to optimize the experimental conditions for developing the gallic acid detection method. Figure 7 shows the effect of pH in a range of 2 to 6 (Figure 7a) and the effect of temperature at 10, 15, 22 and 30 °C (Figure 7b). It is shown that pH 2 and a temperature of 22 °C are the best working conditions.

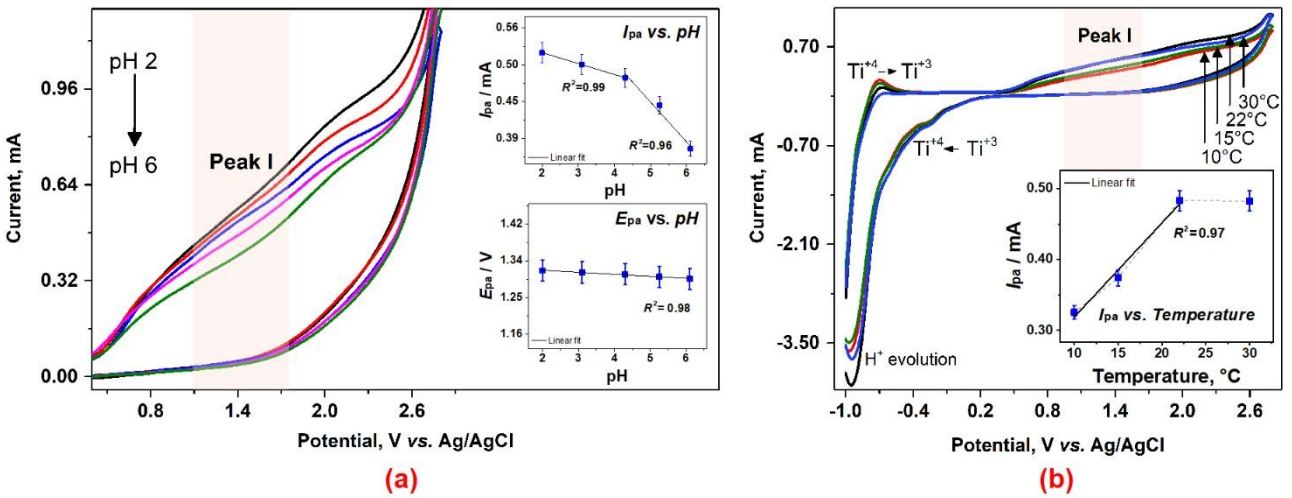

Figure 7. *(a) Effect of pH and (b) temperature on GA (5 mM) detection in 1 M KCl at the Ag-TNA electrode. The insets in (a) show the linear relationship between anodic peak current and anodic peak potential with pH (I_{pa} vs. pH and E_{pa} vs. pH) and (b) between anodic peak current and temperature (I_{pa} vs. temperature)*

The current intensity of peak I decreased with increasing pH (Figure 7a, I_{pa} vs. pH), suggesting reduced electron-transfer efficiency in less acidic media. In parallel, a decrease in anodic peak

potential (Figure 7a, E_{pa} *vs.* pH) was observed as pH increased, consistent with a proton-coupled electron-transfer mechanism [44,45]. This shift reflects changes in the protonation state of the electroactive species and supports the involvement of protons in the first oxidation step. These results indicate that acidic conditions favour the oxidation process and that the electrochemical behaviour of gallic acid is strongly dependent on proton availability. The temperature effect (Figure 7b) exhibits a progressive increase in the anodic peak current (I_{pa}) from 10 to 22 °C, suggesting enhanced mass transport and faster electron transfer kinetics at higher temperatures. However, at 30 °C, the current remained nearly constant compared to 22 °C, indicating the onset of kinetic and surface-related limitation.

The effect of scan rate was also evaluated. The response is shown in Figure 8a, where the voltammograms obtained for each evaluated rate (20, 40, 60, 80, 100, 120, 140 and 160 mV s^{-1}) are compared. The shift of the anodic peak potential (E_{pa}) towards more positive values as the scan rate increases indicates irreversible behaviour of the system, further evidenced by the absence of a reduction peak for gallic acid. Within the 20 to 100 mV s^{-1} range, a linear relationship between anodic peak current and scan rate is observed. At higher rates (>100 mV s^{-1}), deviations from linearity became evident, suggesting limitations in the electrochemical response associated with mass transport and/or charge transfer processes [45]. Therefore, a scan rate of 100 mV s^{-1} was selected as the working parameter for the subsequent analyses, as it provides an optimal balance between well-defined electrochemical behaviour and current intensity. This behaviour is consistent with the results obtained through EIS analyses.

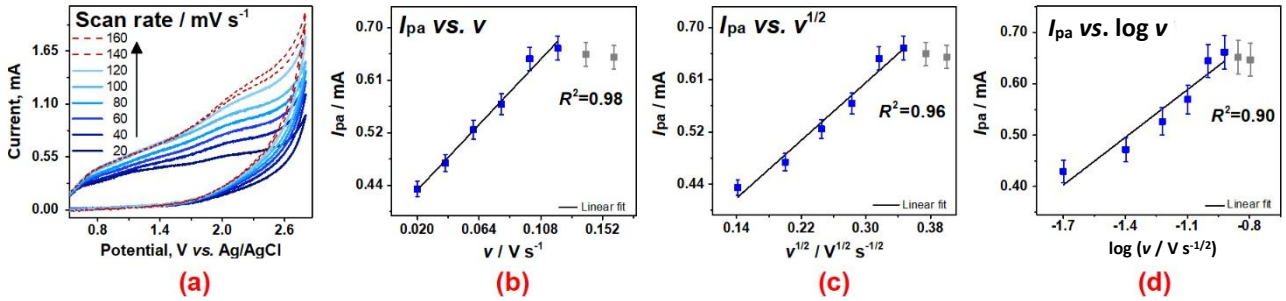

Figure 8. *(a) Effect of scan rate (20, 40, 60, 80, 100, 120, 140 and 160 mV s^{-1}) on CV of 5 mM GA oxidation at Ag-TNA electrode in 1 M KCl, pH 2, 22 °C, (b-d) anodic peak intensity related to different scan rate functions (*v, $v^{1/2}$ *and log* v*, respectively)*

Further analysis of electrochemical kinetics using scan rate studies, presented in Figure 8 (b-d), revealed mixed diffusion and adsorption-controlled behaviour. The anodic peak current (I_{pa}) showed linear relationship with both the square root of the scan rate ($v^{1/2}$), characteristic of diffusion-controlled processes, and the scan rate (v), typical of mechanisms dominated by surface adsorption. This behaviour suggests that the oxidation of gallic acid on the surface of the modified electrode Ag-TNA/Ti simultaneously involves transport from the solution and interaction with active surface sites [2].

The calibration of the electrochemical signal for gallic acid was performed using cyclic voltammetry under optimized conditions, *i.e.* pH 2, temperature of 22 °C, and scan rate of 100 mV s^{-1}. Under these conditions, the selected anodic working signal corresponding to peak I at +1.30 V *vs*. Ag/AgCl exhibited two different linear ranges with different sensitivities, as shown in Figure 9 [2,41].

In the low concentration range "peak I, range I" (0 to 425 µM), an excellent linear correlation was obtained with a coefficient of determination (R^2) of 0.993 and a sensitivity of 219 µA mM^{-1} cm^{-2}. In the second range, "peak I, range II" (565 to 4663 µM), high linearity was also achieved with

R^2 = 0.997 and a sensitivity of 118 µA mM^{-1} cm^{-2}, demonstrating good analytical response even at high concentrations.

From the second linear range of peak I (565 to 4663 µM), the detection limit (LOD) and quantification limit (LOQ) were calculated using the standard equations LOD = 3σ/S and LOQ = 10σ/S, where σ represents the standard deviation of the repeated measurements and S corresponds to the sensitivity of the range considered (118 µA mM^{-1} cm^{-2}). The values obtained were 13.2 µM for the LOD and 43.9 µM for the LOQ, supporting the applicability of the system for quantification at moderate to high concentrations. These results are illustrated in Figure 9b.

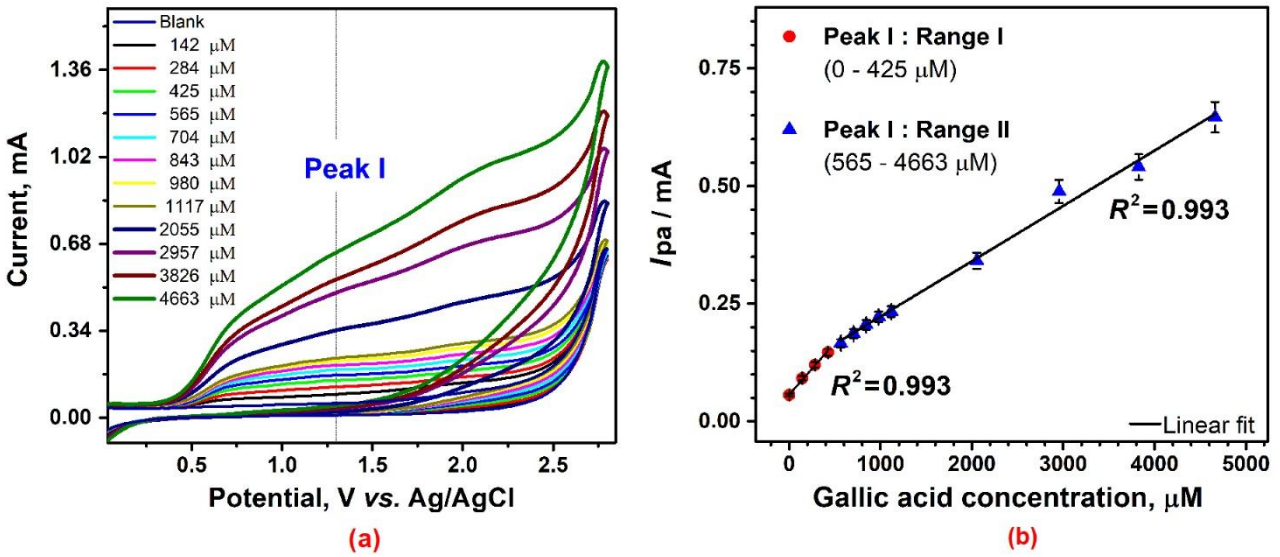

Figure 9. *Concentration test: (a) CVs of different gallic acid concentrations (0 to 4663 µM) at Ag-TNA electrode in 1 M KCl, pH 2, 22 °C, at 100 mV s^{-1}, (b) The relationship between anodic peak intensity and molar concentration of gallic acid (*I_{pa} vs. C*) and the corresponding linear fit*

The validation of the analytical performance of the developed sensor (Figure 10) includes the evaluation of its repeatability, reproducibility, and stability over time. To assess stability over time, the electrodes were stored at room temperature and protected from air. The optimal operational conditions previously described were used for these tests (pH 2, temperature of 22 ° C and scan rate of 100 mV s^{-1}).

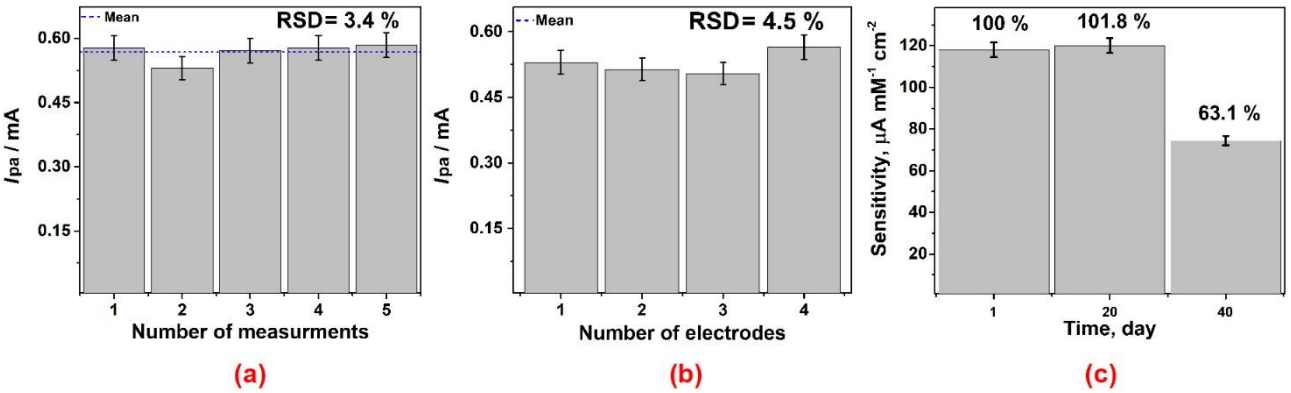

Figure 10. *Accuracy and stability of Ag-TNA electrode in response to 5 mM GA in 1M KCl: (a) repeatability, (b) reproducibility, and (c) long-term stability (shelf life)*

Repeatability (Figure 10a) was evaluated using a single electrode to measure five independent gallic acid solutions at a concentration of 5 mM. The relative standard deviation (RSD) obtained was 3.4 %, indicating good consistency in the electrochemical response under controlled conditions.

Reproducibility (Figure 10b) was determined using four different electrodes, prepared under the same conditions and measuring 5 mM gallic acid solutions. In this case, an RSD of 4.5 % was obtained, reflecting acceptable variation between devices and demonstrating reliability in electrode manufacturing and structural stability across batches.

To evaluate temporal stability or shelf life (Figure 10c), the complete calibration curves (0 to 4663) were repeated at 20 and 40 days after electrode preparation (Figure 11), and the slopes obtained by linear regression were compared with that of day 1 (Figure 9, taken as 100 %) in range II of peak I (565 to 4663 µM) at 20 days, the slope remained virtually unchanged (101.7 %), while at 40 days it decreased significantly (63.4 %), showing a progressive loss of sensitivity in this upper range. Figure 11 provides further details on the stability evolution.

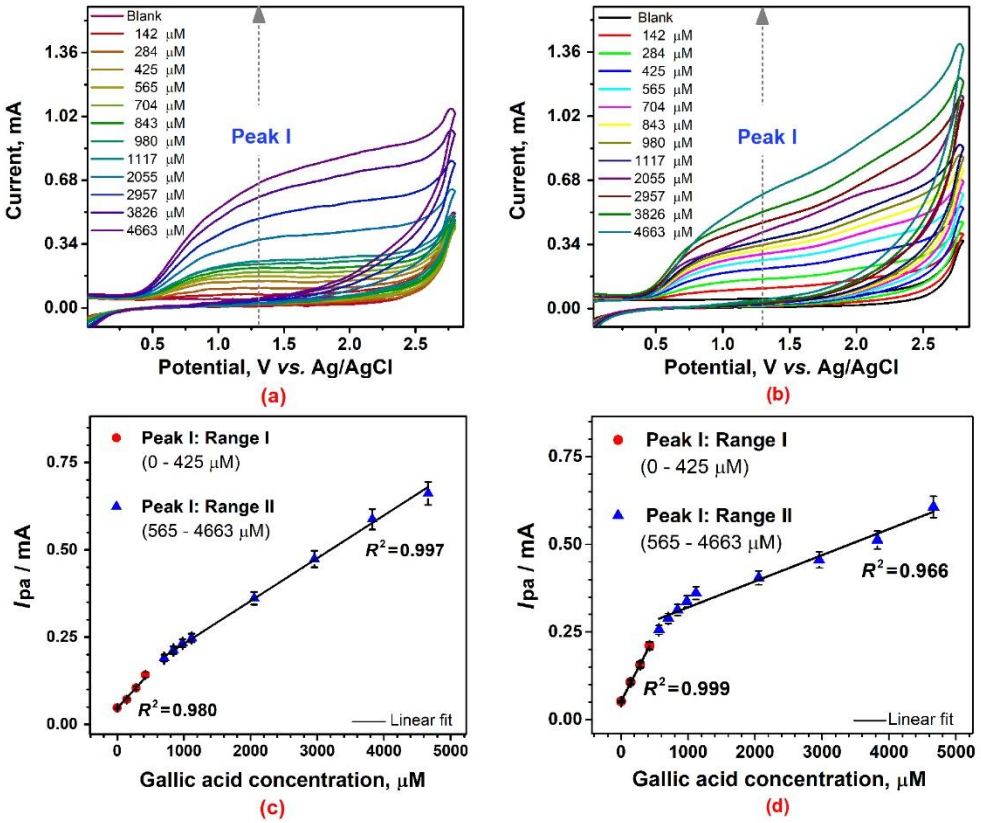

Figure 11. *Long-term stability of the Ag-TNA electrode: (a-b) comparison of CVs obtained in response to the increase in gallic acid concentration (0 to 4663 µM) on day 20, and day 40 after the sensor was manufactured, respectively, and (c-d) the corresponding* I_{pa} *vs. concentration linear adjustments*

From Figure 11, it should be noted that on day 20 (Figures 11a and c), both range I and range II of peak I retained their linearity and sensitivity, with no significant changes. By day 40 (Figure 11b and 11d), range I of peak I not only maintained its linearity but also increased its sensitivity significantly, reaching a value of 371 µA mM^{-1} cm^{-2}. In contrast, range II of the same peak suffered a reduction in both sensitivity and linear fit quality.

Although these variations reflect a loss of overall stability after 20 days, the results also indicate a specific increase in sensitivity, which could be exploited by periodically recalibrating the sensor.

Selectivity towards the analyte of interest is an important aspect in electrode selection, so the sensor's selectivity was evaluated against possible common interferences in real matrices, mainly glucose and ascorbic acid. First, the influence of glucose was analysed in gallic acid: glucose ratios of 1:0, 1:1, 1:10 and 1:100 (Figure 12a). In all cases, no signal attributable to glucose was observed, nor was there any effect on the gallic acid response, suggesting a high tolerance of the sensor to this molecule.

Subsequently, the voltametric response was evaluated in the simultaneous presence of gallic acid and ascorbic acid (AA). The interference effect of AA was evaluated at GA: AA ratios ranging from 1:0 to 1:5 (Figure 12b). For ratios between 1:0.2 and 1:1.0, although an oxidation signal attributable to AA was observed, no significant alteration in the position or intensity of the gallic acid analytical peak (1.3 V) was detected. This indicates that the sensor tolerates ascorbic acid up to equimolar concentration. However, when the concentration of AA exceeded that of GA (≥ 1 : 1.2), a noticeable increase in the current analytical potential was observed, indicating the onset of interference. At higher excess (1:5), the interference became significant. This separation of signals allowed the integrity of the gallic acid analytical signal to be maintained, demonstrating adequate selectivity of the sensor against possible interferents [20].

These results not only highlight the system's specificity for gallic acid but also suggest its potential for developing voltametric sensors with multi-analyte detection capabilities. In more advanced scenarios, studies on the simultaneous quantification of antioxidants in complex samples could be considered, expanding the device's scope for food and nutraceutical applications.

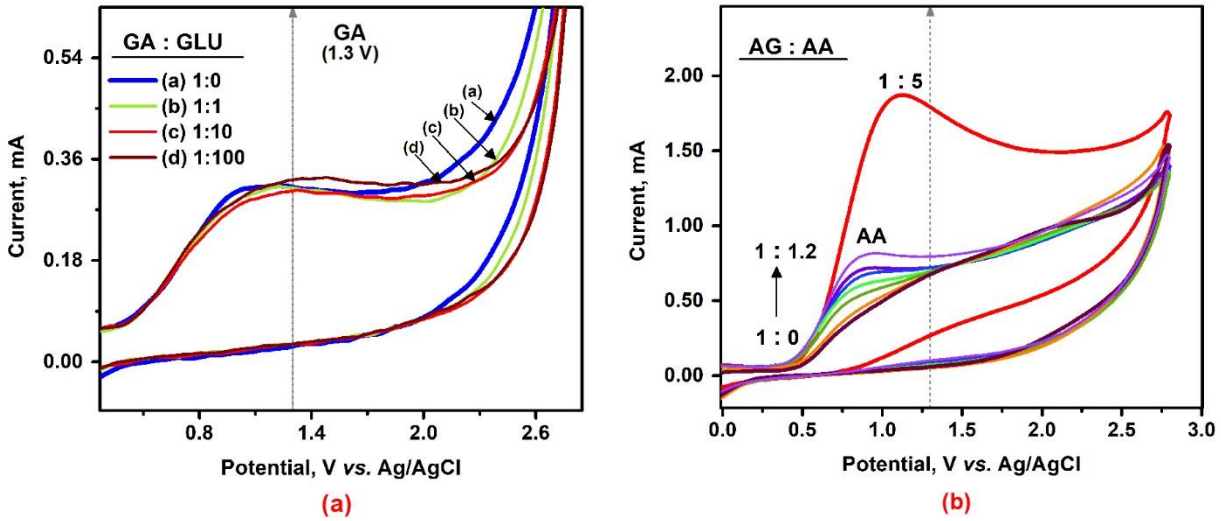

Figure 12. *Interference test: evaluation of gallic acid (GA) selectivity at the Ag-TNA electrode in the presence of (a) glucose (ratio of 1:0, 1:1, 1:10 and 1:100), and (b) ascorbic acid (ratio 1:0, 1:0.2, 1:0.4, 1:0.6, 1:0.8, 1:1, 1:1.2 and 1:5)*

In Table 2, the results obtained in this work are compared with other sensors reported in the literature.

Table 2*. Analytical parameters of some gallic acid electrochemical sensors*

Electrode material	LR, µM	LOD, µM	LOQ, µM	Sensitivity	Stability (long term)	Ref.
Ag-TNA	565-4663 (R^2= 0.997)	13.2	43.9	118 µA mM^{-1} cm^{-2}	No sensitivity loss at 20 days	This work
CS–fFe_2O_3–ERGO/GCE	1 to 100 (R^2= 0.98)	0.13	Not specified	Not specified	Lost 6 % of sensitivity in 1 week	[20]
AgNP/Delph/GCE	0.60 to 8.68	0.28	Not specified	10 µA mM^{-1}	Stable through 1750 s	[46]
Screen printed carbon electrode	100 to 2000 (R^2= 0.993)	33	99 .0	2.808 µA mM^{-1}	Not specified	[2]
CeO_2-Brij® 35/GCE	50 to 2490	11.9	39.6	Not specified	Not specified	[47]

Although the Ag-TNA electrode exhibits a higher LOD, it demonstrates clear advantages, including a substantially wider linear range (LR), higher sensitivity, and outstanding long-term stability. Additionally, its simplified and low-cost fabrication process further highlights the robustness and practical applicability of the Ag-TNA platform compared with previously published electrodes.

Conclusion

In this study, an electrochemical sensor based on a matrix of silver-doped TiO_2 nanotubes was developed and validated for the detection of gallic acid using cyclic voltammetry. The system showed a reliable analytical response over a wide range of concentrations (0 to 4663 µM), with detection and quantification limits suitable for application in the non-alcoholic beverage industry (LOD = 13.2 µM; LOQ = 43.9 µM), and characteristic slopes for each range and oxidation peak. Two linear regions were identified in the first peak (1.30 V), with the high range (565 to 4663 µM) standing out for its robustness (R^2 = 0.997; sensitivity = 118 µA Mm^{-1} cm^{-2}).

The method showed good repeatability (RSD = 3.4 %) and reproducibility (RSD = 4.5 %), as well as remaining stable for 20 days in the linear range of 565 to 4663 µM. However, 40 days after manufacturing, the sensor exhibited alterations in linearity and sensitivity at peak I but remained functional, which could be addressed by periodic recalibration. In addition, the sensor demonstrated good selectivity toward common food-matrix interferents, such as glucose and ascorbic acid, while maintaining the integrity of the gallic acid signal.

Conflict of interest: *The authors declare no conflict of interest.*

Acknowledgments: *Zaira Mora gratefully acknowledges SECIHTI-México for the financial support provided through the doctoral scholarship No. 842308. Instituto de Ciencia Tecnología e Innovación del Estado de Michoacán (ICTI) for its financial support to the project PICIR22-059-C, and Coordinación de la Investigación Científica de la Universidad Michoacana de San Nicolás de Hidalgo financial support. The authors thank Willian Javier Cauich Ruiz and Monica Monserrat Martinez Garcia from the National Laboratory of Nano and Biomaterials (LANNBIO), CINVESTAV–Unidad Mérida, for their assistance with the XPS and Raman measurements.*

Funding: *No funding.*

References

[1] S. Verma, D. Thakur, C. M. Pandey, D. Kumar, Recent Prospects of Carbonaceous Nanomaterials-Based Laccase Biosensor for Electrochemical Detection of Phenolic Compounds, *Biosensors* **13** (2023) 305. https://doi.org/10.3390/bios13030305

[2] M. Badea, F. di Modugno, L. Floroian, D. M. Tit, P. Restani, S. Bungau, C. Iovan, G. E. Badea, L. Aleya, Electrochemical strategies for gallic acid detection: Potential for application in clinical, food or environmental analyses, *Science of The Total Environment* **672** (2019) 129-140. https://doi.org/10.1016/j.scitotenv.2019.03.404

[3] B. Brunetti, Electrochemical Sensors and Biosensors for the Determination of Food Nutritional and Bioactive Compounds: Recent Advances, *Sensors* **24** (2024) 6588. https://doi.org/10.3390/s24206588

[4] S. Falahi, S. Falahi, M. Zarejousheghani, H. Ehrlich, Y. Joseph, P. Rahimi, Electrochemical Sensing of Gallic Acid in Beverages Using a 3D Bio-Nanocomposite Based on CarbonNanotubes/Spongin-Atacamite, *Biosensors* **13** (2023) 262. https://doi.org/10.3390/bios13020262

[5] P. Yammine, H. El-Nakat, R. Kassab, A. Mansour, B. El Khoury, D. Koumeir, Z. Matar, A. Chmayssem, Recent Advances in Applied Electrochemistry: A Review, *Chemistry* **6** (2024) 407-434. https://doi.org/10.3390/chemistry6030024

[6] M. A. Darwish, W. Abd-Elaziem, A. Elsheikh, A. A. Zayed, Advancements in nanomaterials for nanosensors: a comprehensive review, *Nanoscale Advances* **6** (2024) 4015-4046. https://doi.org/10.1039/D4NA00214H

[7] N. German, A. Ramanaviciene, J. Voronovic, A. Ramanavicius, Glucose biosensor based on graphite electrodes modified with glucose oxidase and colloidal gold nanoparticles, *Microchimica Acta* **168** (2010) 221-229. https://doi.org/10.1007/s00604-009-0270-z
[8] Annu, S. Sharma, R. Jain, A. N. Raja, Review—Pencil Graphite Electrode: An Emerging Sensing Material, *Journal of The Electrochemical Society* **167** (2020) 037501. https://doi.org/10.1149/2.0012003JES
[9] Q. Yuan, Z. Zhang, L. Li, Electrochemical Sensor Based on Glassy Carbon Electrode Modified by Palladium Doped ZnO Nanostructures for Glucose Detection, *International Journal of Electrochemical Science* **15** (2020) 5245-5254. https://doi.org/10.20964/2020.06.80
[10] M. Ghadirinataj, S. K. Hassaninejad-Darzi, H. Emadi , An electrochemical nanosensor for simultaneous quantification of acetaminophen and acyclovir by ND@Dy_2O_3-IL/CPE, *Electrochimica Acta* **450** (2023) 142274. https://doi.org/10.1016/j.electacta.2023.142274
[11] M. Zamani, C. M. Klapperich, A. L. Furst, Recent advances in gold electrode fabrication for low-resource setting biosensing, *Lab on a Chip* **23** (2023) 1410-1419. https://doi.org/10.1039/D2LC00552B
[12] N. Mecheri, M. Benounis, H. Barhoumi, New modified selective platinum electrode based on poly (ethylene glycol) for Iron (III) detection in real water, *Sensor Review* **37** (2017) 436-443. https://doi.org/10.1108/SR-01-2017-0020
[13] H. Silah, C. Erkmen, E. Demir, B. Uslu, Modified indium tin oxide electrodes: Electrochemical applications in pharmaceutical, biological, environmental and food analysis, *Trends in Analytical Chemistry* **141** (2021) 116289. https://doi.org/10.1016/j.trac.2021.116289
[14] A. T. Lawal, Recent developments in electrochemical sensors based on graphene for bioanalytical applications, *Sensing and Bio-Sensing Research* **41** (2023) 100571. https://doi.org/10.1016/j.sbsr.2023.100571
[15] J. Hu, Z.-y. Wang, C.-c. Li, C.-y. Zhang, Advances in single quantum dot-based nanosensors, *Chemical Communications* **53** (2017) 13284-13295. https://doi.org/10.1039/C7CC07752A
[16] D. Nunes, A. Pimentel, A. Gonçalves, S. Pereira, R. Branquinho, P. Barquinha, E. Fortunato, R. Martins, Metal oxide nanostructures for sensor applications, *Semiconductor Science and Technology* **34** (2019) 043001. https://doi.org/10.1088/1361-6641/ab011e
[17] M. Pimpilova, A brief review on methods and materials for electrode modification: electroanalytical applications towards biologically relevant compounds, *Discover Electrochemistry* **1** (2024) 12. https://doi.org/10.1007/s44373-024-00012-8
[18] M. Khanchoupan, A. Pishevar, D. Souri, R. Yusofvand, Z. Dabirifar, Platinum-based electrochemical sensors for glucose detection: a mini-review, *Synthesis and Sintering* **4** (2024) 292-303. https://doi.org/10.53063/synsint.2024.44252
[19] S. Malik, J. Singh, R. Goyat, Y. Saharan, V. Chaudhry, A. Umar, A. A. Ibrahim, S. Akbar, S. Ameen, S. Baskoutas, Nanomaterials-based biosensor and their applications: A review, *Heliyon* **9** (2023) 19929. https://doi.org/10.1016/j.heliyon.2023.e19929
[20] F. Gao, D. Zheng, H. Tanaka, F. Zhan, X. Yuan, F. Gao, Q. Wang, An electrochemical sensor for gallic acid based on Fe_2O_3/electro-reduced graphene oxide composite: Estimation for the antioxidant capacity index of wines, *Materials Science and Engineering C* **57** (2015) 279-287. https://doi.org/10.1016/j.msec.2015.07.025
[21] M. Guo, G. Zhu, Y. Mishchencko, A. Butenko, V. Kovalenko, T. Rozhkova, H. Zhao, Highly sensitive electrochemical detection of gallic acid in tea samples by using single-walled carbon nanotubes@silica dioxide nanoparticles decorated electrode, *International Journal of Electrochemical Science* **18** (2023) 100291. https://doi.org/10.1016/j.ijoes.2023.100291
[22] L. Bertel, D. A. Miranda, J. M. García-Martín, Nanostructured Titanium Dioxide Surfaces for Electrochemical Biosensing, *Sensors* **21** (2021) 6167. https://doi.org/10.3390/s21186167

[23] X. Hou, Active Area of Anodic TiO_2 Nanotube Arrays in Photo and Electrochemical Energy Storage Devices, *ACS Applied Energy Materials* **5** (2022) 12869-12873. https://doi.org/10.1021/acsaem.2c02492
[24] T. S. Dhahi, A. K. Yousif, O. E. Tayfour, A. Mubarakali, A. S. Alqahtani, A. E. Tayfour, M. E. Elobaid, T. Adam, S. C. Gopinath, Advances in nano sensors for monitoring and optimal performance enhancement in photovoltaic cells, *iScience* **27** (2024) 109347. https://doi.org/10.1016/j.isci.2024.109347
[25] Y. Liu, Y. Yang, Recent Progress of TiO_2-Based Anodes for Li Ion Batteries, *Journal of Nanomaterials* (2016) 8123652. https://doi.org/10.1155/2016/8123652
[26] D. Matsunami, K. Yamanaka, T. Mizoguchi, K. Kojima, Comparison of photodegradation of methylene blue using various TiO_2 films and WO_3 powders under ultraviolet and visible-light irradiation, *Journal of Photochemistry & Photobiology A: Chemistry* **369** (2019) 106-114. https://doi.org/10.1016/j.jphotochem.2018.10.020
[27] C. O. Chikere, E. F. Hobben, H. Nadimul, P. Kong-Thoo-Lin, C. Fernandez, Electroanalytical determination of gallic acid in red and white wine samples using cobalt oxide nanoparticels-modified carbon-paste electrodes, *Microchemical Journal* **160** (2021) 105668. https://doi.org/10.1016/j.microc.2020.105668
[28] É. M. Margalho, O. Lima, Jr., C. Alfonso, I. R. Segundo, S. J. Landi, E. Freitas, M. F. M. Costa, J. Carneiro, Iron-Modified Nano-TiO_2: Comprehensive Characterization for Enhanced Photocatalytic Properties, *Photonics* **11** (2024) 888. https://doi.org/10.3390/photonics11090888
[29] K. Indira, U. K. Mudali, T. Nishimura, N. Rajendran, A Review on TiO_2 Nanotubes: Influence of Anodization Parameters, Formation Mechanism, Properties, Corrosion Behavior, and Biomedical Applications, *Journal of Bio- and Tribo-Corrosion* **1** (2015) 28. https://doi.org/10.1007/s40735-015-0024-x
[30] H. Yoo, M. Kim, Y.-T. Kim, K. Lee, J. Choi, Catalyst-Doped Anodic TiO_2 Nanotubes: Binder-Free Electrodes for (Photo)Electrochemical Reactions, *Catalysts* **8** (2018) 555. https://doi.org/10.3390/catal8110555
[31] H. Zhou, Y. Zhang, Electrochemically Self-Doped TiO_2 Nanotube Arrays for Supercapacitors, *The Journal of Physical Chemistry C* **118** (2014) 5626-5636. https://doi.org/10.1021/jp4082883
[32] D. Luca, M. Dobromir, G. Stoian, A. Ciobanu, M. Luca, Porous-Wall Titania Nanotube Array Layers: Preparation and Photocatalytic Response, *Nanomaterials* **13** (2023) 3000. https://doi.org/10.3390/nano13233000
[33] X. Jiang, Q. Lin, Y. Zhang, K. Dong, Y. Zhang, Y. Shi, TiO_2 nanotube arrays: hydrothermal fabrication and photocatalytic activities, *Journal of Materials Science: Materials in Electronics* **28** (2017) 12509-12513. https://doi.org/10.1007/s10854-017-7073-5
[34] E. C. R. Lopez, J. D. Ocon,d J. V. D. Perez, Synthesis of Silver-Doped Titanium Dioxide Nanotubes by Single-Step Anodization for Enhanced Photodegradation of Acid Orange 52, *Materials Science Forum* **950** (2019) 149-153. 10.4028/www.scientific.net/MSF.950.149
[35] S. P. Lim, M. M. Shahid, P. Rameshkumar, N. M. Huang, L. Che, Amperometric detection of hydrogen peroxide and its density functional theory for adsorption on Ag/TiO_2 nanohybrid, *Journal of Materials Science: Materials and Electronics* **31** (2020) 6017-6026. https://doi.org/10.1007/s10854-020-03153-9
[36] M. G. Garnica-Romo, Z. Mora-Mora, J. J. Alvarado-Gil, H. E. Martínez-Flores, Electrochemical nanosensor based on Ag-doped TiO_2 nanotubes for detecting ascorbic acid, *International Journal of Electrochemical Science* **19** (2024) 100481. https://doi.org/10.1016/j.ijoes.2024.100481

[37] T. Berger, D. Monllor-Satoca, M. Jankulovska, T. Lana-Villarreal, R. Gómez, The Electrochemistry of Nanostructured Titanium Dioxide Electrodes, *ChemPhysChem* **13** (2012) 2824-2875. https://doi.org/10.1002/cphc.201200073

[38] S. Sen, S. Mahanty, S. Roy, O. Heintz, S. Bourgeois, D. Chaumont, Investigation on sol-gel synthesized Ag-doped TiO_2 cermet thin films, *Thin Solid Films* 474 (2005) 245-249. https://doi.org/10.1016/j.tsf.2004.04.004

[39] P. V. Viet, B. T. Phan, D. Mott, S. Maenosono, T. T. Sang, C. M. Thi, L. V. Hieu, Silver nanoparticle loaded TiO_2 nanotubes with high photocatalytic and antibacterial activity synthesized by photoreduction method, *Journal of Photochemistry and Photobiology A: Chemistry* **352** (2018) 106-112. https://doi.org/10.1016/j.jphotochem.2017.10.051

[40] D. A. H. Hanaor, C. C. Sorrell, Review of the anatase to rutile phase transformation, *Journal of Materials Science* **46** (2011) 855-874. https://doi.org/10.1007/s10853-010-5113-0

[41] S. Lisnund, V. Blay, K. Chansaenpak, P. Pinyou, Voltammetric Determination of Gallic Acid with a Glassy Carbon Electrode modified with Reduced Graphene Oxide, *International Journal of Electrochemical Science* **15** (2020) 7214-7227. https://doi.org/10.20964/2020.08.06

[42] A. Escarpa, Food Electroanalysis: Sense and Simplicity, *The Chemical Record* **12** (2012) 72-91. https://doi.org/10.1002/tcr.201100033

[43] I. Novak, M. Šeruga, Š. Komorsky-Lovrić, Electrochemical Characterization of Epigallocatechin Gallate Using Square-Wave Voltammetry, *Electroanalysis* **21** (2009) 1019-1025. https://doi.org/10.1002/elan.200804509

[44] S. Duzmen, A. K. Baytak and M. Aslanoglu, A novel voltammetric platform composed of poly(aminopyrazine), ZrO_2 and CNTs for a rapid, sensitive and selective determination of ascorbic acid in pharmaceuticals and food samples, *Materials Chemistry and Physics* **252** (2020) 123170. https://doi.org/10.1016/j.matchemphys.2020.123170

[45] M. Chen, H. Lv, X. Li, Z. Tian, X. Ma, Determination of Gallic Acid in Tea by a Graphene Modified Glassy Carbon Electrode, *International Journal of Electrochemical Science* **14** (2019) 4852-4860. https://doi.org/10.20964/2019.05.23

[46] M. Ghaani, N. Nasirizadeh, S. A. Y. Ardakani, F. Z. Mehrjardi, M. Scampicchio, S. Farris, Development of an electrochemical nanosensor for the determination of gallic acid in food, *Analytical Methods* **8** (2016) 1103-1110. https://doi.org/10.1039/C5AY02747K

[47] G. K. Ziyatdinova, E. R. Ziganshina, P. N. Cong, H. C. Budnikov, Determination of the Antioxidant Capacity of the Micellar Extracts of Spices in Brij 35 Medium by Differential Pulse Voltammetry, *Journal of Analytical Chemistry* **71** (2016) 573-580. https://doi.org/10.1134/S1061934816060174